Galles, D., and Beckermann, C., "Distortion of a Steel Cylinder Casting with a Core," in Proceedings of the 67th SFSA Technical and Operating Conference, Paper No. 5.8, Steel Founders' Society of America, Chicago, IL, 2013.

Distortion of a Steel Cylinder Casting with a Core

D. Galles and C. Beckermann
Mechanical and Industrial Engineering Department, University of Iowa, Iowa City, Iowa 52242, USA

Abstract

Casting distortions, which are unwanted dimensional changes resulting from stresses during solidification and cooling, are studied through a series of in situ casting trials in which a low-carbon steel cylinder with a core is produced. The inner and outer diameters of the cylinder are continuously measured throughout the casting process; the measurements show that thermal expansions (of both the outer mold and core) have an immediate impact on the final casting dimensions. Additional measurements are taken with a digital calipers after shakeout, from which pattern allowances are subsequently calculated. The largest distortions occur at the mid-height of the inner diameter, which is the last part of the casting to solidify, and thus, most vulnerable to stresses. Preliminary finite element simulations are performed, in which thermal strains are predicted in the core and casting; the results suggest 1) the thermal expansion coefficient of the mold, which was previously measured with a dilatometer, is likely incorrect and must be studied further, and 2) shortly after solidification is complete, all measured dimensional changes in the casting are due to thermal contractions of the steel.

1. Introduction

The final dimensions of a steel casting are commonly calculated (as a first estimation) using the patternmaker's shrink, for which an over-sized pattern is built to account for thermal contractions. While these contractions (i.e., thermal strains) are well-known and predicted accurately, they unfortunately also lead to unwanted stresses and distortions (i.e., plastic strains) resulting from mechanical interactions at the mold-metal interface. As a result, deviations between the predicted and actual final dimensions necessitate that 1) the pattern is re-designed, or 2) post-casting operations (machining, grinding, welding) are performed to add or remove material. In either case, costly and time-consuming effort is needed to meet dimensional specifications.

In order to avoid these problems, the mechanical behavior of the steel must be considered. In recent years, advanced constitutive (stress-strain) models for austenitic steel have been developed to predict stresses and distortions during solidification and cooling. For early studies, these models were calibrated with high-temperature stress-strain data from the uni-axial tests of Wray [1] and Suzuki et al. [2], in which reheated steel specimens were annealed for a period and plastically deformed under isothermal conditions (i.e., data was collected in a controlled environment). However, Galles et al. [3] showed that models calibrated with these data are unable to predict distortions in an industrial casting environment and should instead use data from in situ casting experiments.

In addition to the mechanical behavior of the steel, the properties of the sand mold also affect the final casting dimensions, namely in two ways; first, mold expansion

(immediately after pouring) displaces the molten steel from the mold cavity into the pouring cup to reduce the casting volume. Second, internal molds (i.e., cores) constrain the casting from free contraction to introduce stresses and distortions. Therefore, deformation models of both the steel and mold are necessary to accurately predict final casting dimensions.

The aim of the present work is to study the effect a core has on the final dimensions of a low-carbon steel casting through a series of experiments. The results are then analyzed and compared with preliminary simulations, which will show the times and casting locations where the core has the greatest impact the final dimensions.

For the experiments, a set of in situ casting trials are performed in which a thick-walled cylinder is produced. The inner and outer diameters of the cylinder are measured continuously during solidification and cooling; in addition, measurements are taken before casting and after shakeout to determine pattern allowances at several casting locations. Temperatures are also measured in the casting and mold.

Next, using thermal simulation software (MAGMAsoft [4]), temperature fields are calculated and validated by matching experimental and simulated temperatures. These results, as well as the temperature-dependent thermal expansion coefficients of the casting and mold, are then exported to a finite element software package (ABAQUS [5]), which calculates the thermal strains in the casting and mold throughout solidification and cooling. Because this study is ongoing, no distortions are predicted at this time and hence, no mechanical model is included. However, the thermal strain results alone will provide powerful insight of the core's effect on the final casting dimensions.

2. Description of Experiments

2.1 Introduction

In order validate a computational model, the experiments should represent the harsh conditions encountered in an industrial casting process, i.e., data should be collected from in situ experiments. Therefore, an experiment was designed to continuously measure displacement throughout solidification and cooling resulting from the combined effect of core expansion and casting contraction. In this section, the experimental setup and casting procedure are thoroughly explained, followed by presentation of the experimental results.

2.2 Experimental Setup

The casting geometry, shown in Figure 1, is a thick-walled cylinder, with a nominal height, inner diameter, and outer diameter of 101.6 mm (4 inches), 50.8 mm (2 inches), and 127.0 mm (5 inches), respectively. The experimental schematic at the casting mid-plane and CAD drawing are shown in Figures 2 and 3, respectively. Referring to the schematic, the inner and outer diameters of the cylinder were continuously measured throughout solidification and cooling with LVDT's (Linear Variable Differential Transformer). LVDT's 1 and 3 were added together to measure the inner diameter of the cylinder, whereas LVDT's 2 and 4 measured the outer diameter. While the outer diameter measurements were taken at the mid-height of the cylinder, it is obvious from the schematic that both inner diameter LVDT measurements could not be

taken at the same height. Therefore, one measurement was taken 5 mm above the cylinder mid-height, while the other was taken 5 mm below. In order to transmit the displacement from the casting, a 3 mm diameter quartz rod was connected at one end to the LVDT, while the other end was inserted 3-5 mm into the mold cavity. While quartz is a suitable material to use in this application because of its high melting point and relatively low thermal expansion, it is also extremely brittle. The quartz rods frequently broke during preliminary experiments due to the build-up of compressive stresses as the casting cooled. To alleviate this problem, protective metal sleeves were inserted over the ends of the quartz rods inside the mold cavity. The sleeves were constructed from 5/16 in. diameter threaded steel rod and cut to 10 mm lengths, through which a 3.5 mm hole was drilled axially. Additionally, the diameter of one end was bored to 6 mm and a depth of 5 mm. Then, using an oxy-acetylene torch, one end of the quartz rod was heated and bulged into a spherical shape. The protective sleeve was inserted over the non-bulged end of the quartz rod and slid to the other end, where the bulged end (of the quartz rod) was seated inside the bored end (of the sleeve); during pouring, the molted steel was assumed to immediately freeze over the protective sleeve; therefore, any change in the inner diameter (due to mold expansion or cylinder contraction) would be translated by the quartz rod and measured by the LVDT. Additionally, to measure the inner diameter, it was necessary for the quartz rods to pass through cylinder wall; therefore, to provide a pathway in which the displacement could be transmitted to the LVDT's, the rods were inserted through quartz tubes that traversed the mold cavity.

In addition to the displacement measurements, temperatures were also measured at several locations; type K thermocouples were inserted into the cope and drag near the mold-metal interface. A type B thermocouple was encased in a quartz tube and inserted into the mold cavity to measure the temperature of the steel during solidification and cooling. The thermocouple placement and mold dimensions are shown in Figure 4.

The mold boxes and pattern were built from wood. The cope and drag were separated by a horizontal parting plane, shown in Figure 2. In order to avoid drilling holes through the solidified molds (to insert the thermocouples and quartz rods), holes were drilled in the mold box, through which steel rods were inserted into the pattern before filling the mold box with bonded sand. After the molds hardened, the steel rods, mold box, and pattern were removed, and the measurement hardware was inserted at the appropriate locations.

To build the molds and cores, Unimin™ IC55 silica lake sand was bonded with a phenolic urethane no-bake (PUNB) binder system and mixed in a Klein™ mixer. The binder accounted for 1.25% of the total mold weight and was mixed using a 55:45 ratio of Part 1 (Pep Set 1000) to Part 2 (Pep Set 2000). The chemical reaction was accelerated with a catalyst (Pep Set 3501) based on 6% of binder weight.

Experimental data was collected using an IOtech model 3005 Personal DAQ system connected to a laptop computer and acquired with DASYLab software; the data was sampled at a rate of 2 Hz.

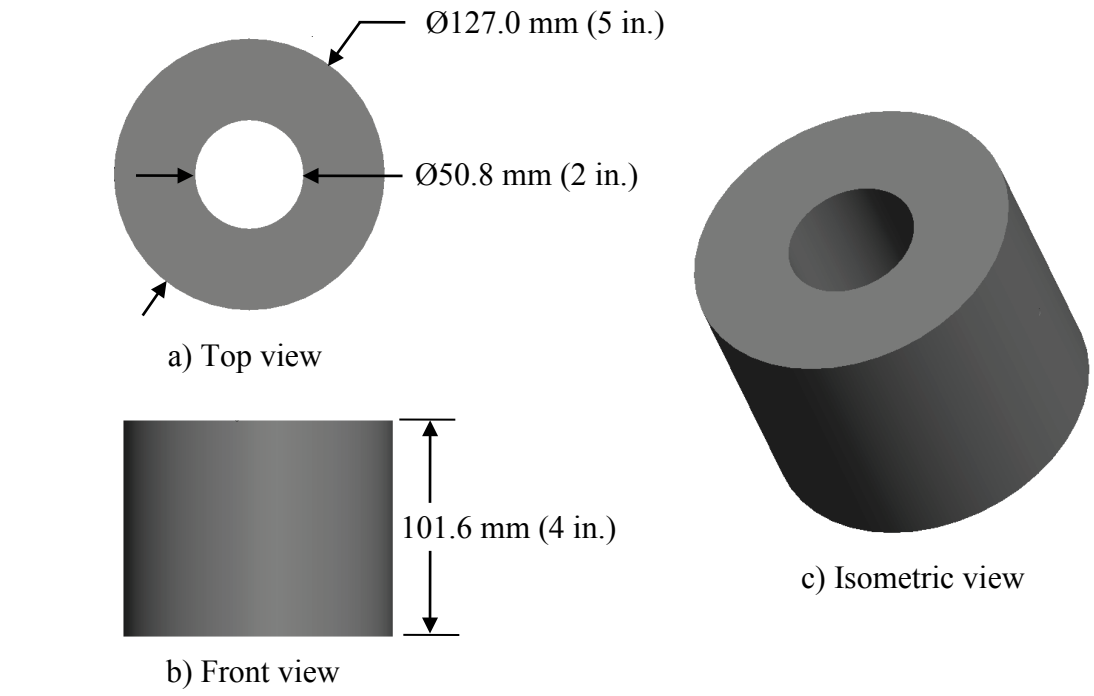

Figure 1. Cylinder nominal dimensions.

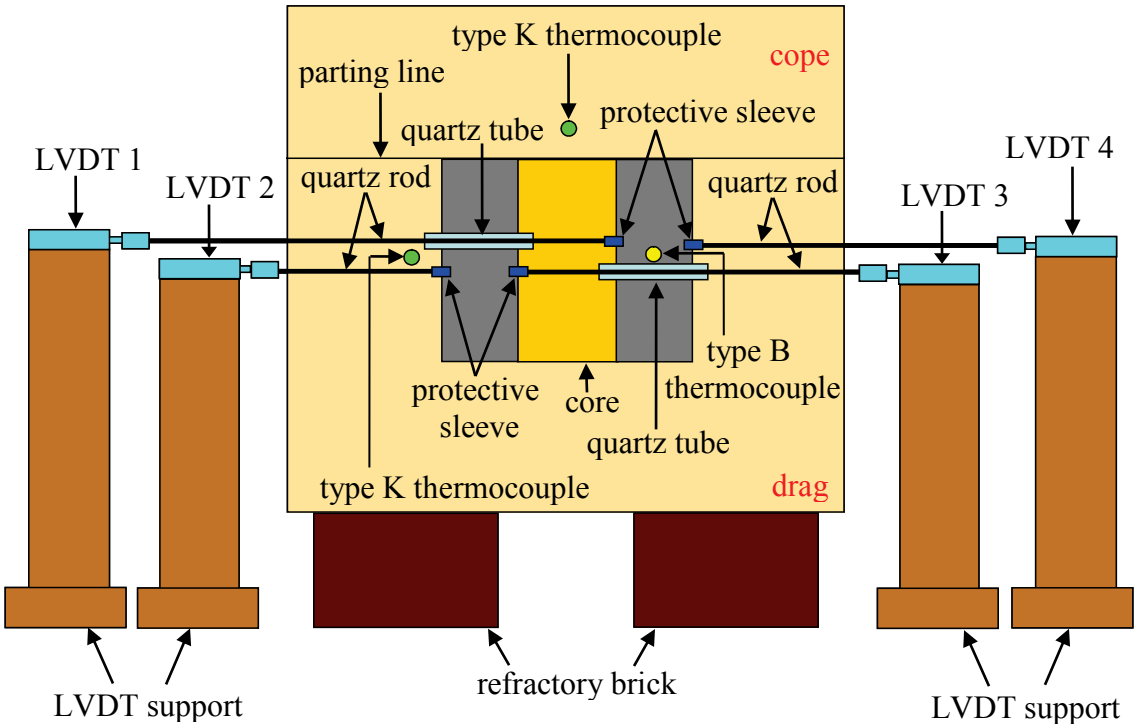

Figure 2. Schematic of experimental setup at mid-plane.

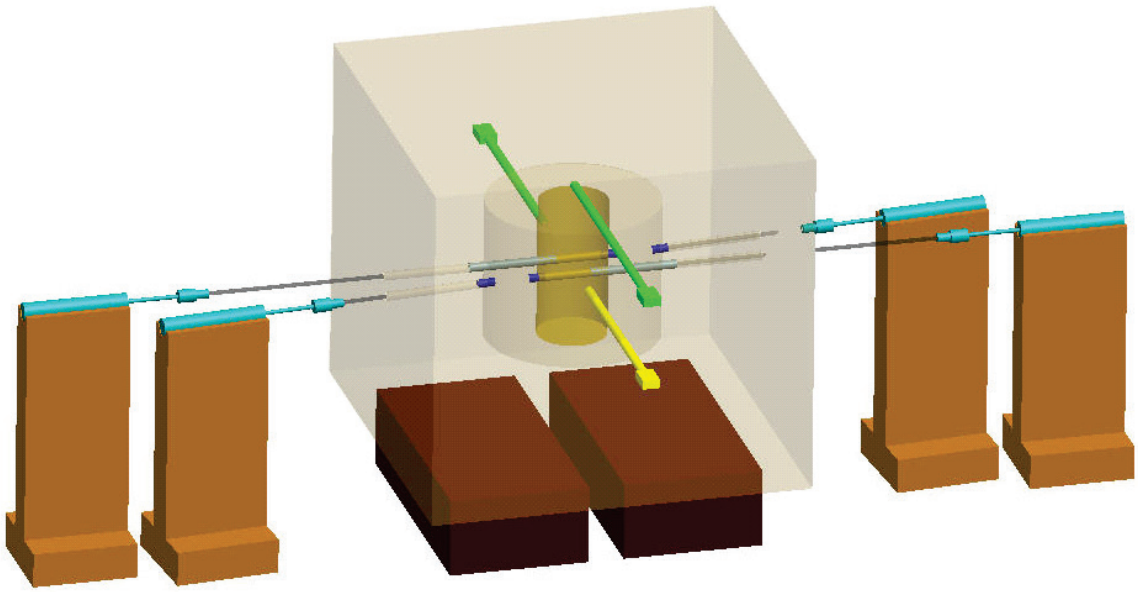

Figure 3. CAD drawing of experimental setup.

2.3 Casting Procedure

Experimental casting trials were performed at the University of Northern Iowa's Metal Casting Center. The target chemistry was ASTM A216 grade WCB carbon steel. The castings were poured from a 250 lb heat and prepared in an induction furnace. Before pouring, the molten steel was heated to approximately 1700°C. In order to protect the sensitive measurement equipment, the molten steel was transmitted from a large ladle to a smaller, hand-held ladle and subsequently poured into the mold cavity. Instead of using a pouring cup to fill the casting, the cope was removed and the liquid metal was poured directly into the mold cavity, after which the cope was immediately placed on top of the drag. This methodology was chosen to eliminate any mechanical interactions between the casting and mold at the mold-metal interface near the sprue and pouring cup; also, in the absence of a pouring cup, the cooling is essentially symmetric along the circumference, which is beneficial when performing simulations (i.e., symmetry boundary conditions can be used to reduce computational times). The castings were poured within four hours after building the molds. Immediately before pouring, any slag was removed from the ladle.

Two experiments were performed, from which a total of six castings were produced (3 castings from each experiment). Due to a limited number of LVDT's, only three displacement measurements could be taken during each experiment. Because the inner diameter quartz probes were most susceptible to failure, two inner diameter measurements and one outer diameter measurement were recorded; the inner and outer diameter measurements were taken from the first casting, while only the inner diameter was measured from the second casting. For the third casting, no LVDT measurements were taken (only temperatures were recorded). A summary of the LVDT allocation for all castings is provided in Table 1, and the casting chemistry for each experiment is listed in Table 2.

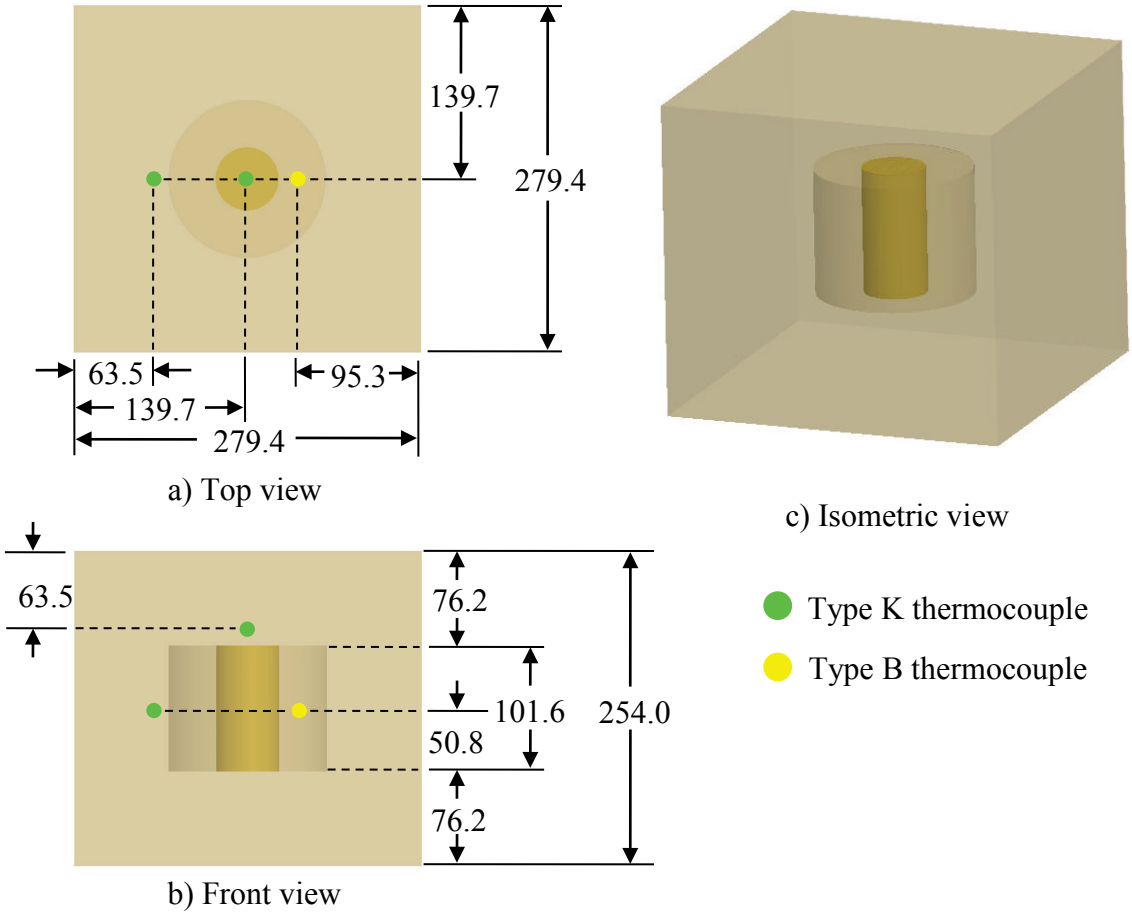

Figure 4. Nominal mold dimensions and thermocouple placement. All units in mm.

Table 1. LVDT allocation. Due to a limited number of LVDT's, only two inner diameter and one outer diameter measurement could be taken during each experiment.

		LVDT Measurements	
	Experiment	Inner Diameter	Outer Diameter
Cylinder 1	1	Yes	Yes
Cylinder 2	1	Yes	No
Cylinder 3	1	No	No
Cylinder 4	2	Yes	Yes
Cylinder 5	2	Yes	No
Cylinder 6	2	No	No

Table 2. Casting Chemistry. The target chemistry was ASTM 216 grade WCB carbon steel.

	Casting Chemistry								
	%C	%Si	%Mn	%P	%S	%Cr	%Al	%Cu	%Fe
Experiment 1	0.27	0.64	0.59	0.021	0.015	0.14	0.069	0.08	bal.
Experiment 2	0.34	1.10	0.68	0.021	0.015	0.92	0.085	0.09	bal.

2.4 Experimental Results

In order to view the occurrence of different events during solidification and cooling, the measured displacements and temperatures are plotted as functions of time on several time scales termed "Large" (40000 s), "Medium" (5000 s) and "Small" (1000 s). In addition, the temperatures recorded in the steel are also shown on a "Very Small" time scale (100 s). The reference time (t = 0 s) coincides with the time when the molten steel was first poured into the mold.

Temperature results from the thermocouple in the steel (termed T_{steel}) are shown in Figure 5. While all temperatures follow the same cooling trend (seen on the Large time scale), differences in experimental conditions (i.e., pouring temperature, casting chemistry) created (slight) variances between the steel temperatures of each casting; these variations are most notable on the Small and Very Small time scales, shown in Figures 5(c) and 5(d), respectively.

The evolution of the temperature curves is summarized by the explanation of several events. Immediately after pouring, the steel temperature increases to a maximum of approximately 1515°C after 20 s (shown in Figure 5(d)) before rapidly decreasing to the liquidus temperature (T_{liq}), after which the liberation of latent heat reduces the cooling rate to nearly zero (i.e., the temperature curves are almost flat). Therefore, the liquidus temperature is experimentally determined at this arrest. The average liquidus temperature for all experiments was 1491°C. All temperature curves showed a similar peak after (approximately) 20 s except the Cylinder 2 casting, which was likely due to a lower pouring temperature. However, because the thermocouples in the steel require several seconds (20-30) to measure the actual temperature (after which the molten steel has considerably cooled), the actual pouring temperature is always higher than the measurement. Therefore, Cylinder 2 was likely poured well above the liquidus temperature but could not measure a superheat due to the physical limitations of the thermocouples.

The solidus temperature (T_{sol}), which represents the end of the solidification period, is experimentally determined at the temperature of the maximum cooling rate. The cooling rate curves, shown in Figure 10, are calculated as the temperature change per time step and plotted as functions of measured temperature. For the present study, a solidus temperature of 1395°C was chosen as a representative value for all experiments.

Below the solidus temperature, the steel cools monotonically until the solid-state phase transformation (from austenite to pearlite and proeutectoid ferrite), which causes

another temperature arrest at approximately 675°C (seen at approximately 3500 s in Figure 5(b)). After the solid-state transformation, the casting continues to cool monotonically to room temperature.

Temperature results for the drag and cope are shown in Figures 11 and 12, respectively. As with the steel temperatures, the measurements appear to be similar on the Large time scales, as the curves essentially lie on top of each other. However, variations can be seen between individual casting temperatures on the Medium and Small time scales, particularly for the cope. As previously explained, the castings were poured directly into the mold cavity, after which the cope was placed on top of the drag. As a result of this filling method, the mold cavity could only be filled a few millimeters from the top of the drag (to avoid spilling molten steel). Therefore, after the cope was placed on top of the drag, an air gap remained between the casting and cope, whose thickness varied between castings; This variation significantly affected the heat transfer between the casting and cope, which caused variations in the cope temperatures at early times. The smaller variations seen in the drag temperatures (on the Small time scale) are likely due to slight differences in thermocouple placement.

The LVDT results for the inner diameter are shown in Figure 13. The quartz probes failed in the Cylinder 1 and Cylinder 2 castings, leaving only measurements from Cylinders 4 ("inner 1" curve) and 5 ("inner 2" curve). The change in the inner diameter is plotted as a function of time; a positive slope reflects core expansion. The Small time scale, shown in Figure 13(c), shows a rapid expansion of the inner diameter to approximately 1 mm at 100 s, after which the curves continue to increase, albeit at a slower rate. After 400 s, the inner diameter begins to decrease with time, as thermal contraction of the cylinder decreases the inner diameter. It should be noted that any variation between the measurements occurs in the first 400 s, after which both inner diameter curves are essentially parallel. Referring back to the Small time scale of the steel temperatures (Figure 9(c)), it can be seen that solidification was complete for all experiments after 400 s. This suggests that before solidification, the semi-solid casting has very little strength, and the measured change in the inner diameter is significantly affected by core expansion. The parallel curves may be an indicator that the dimensional changes after 400 s are the result of free contraction in the cylinder; a thermal strain simulation of the cylinder will either confirm or reject this hypothesis. Furthermore, the initial core expansion likely occurs before the casting has reached coherency; as a result, no stresses are induced because the steel has no strength. At some time, however, the steel reaches coherency and begins to resist core expansion, after which distortions are possible. Although there is no experimental evidence as to when this may occur, future stress simulations will provide better insight to the time when distortions are likely.

The inner diameter continues to decrease with time until 3500 s, where it experiences an increase until 4000 s; this expansion is due to the solid-state transformation. Upon further cooling, the change in the inner diameter decreases to nearly zero at room temperature, resulting in very little net change of the measured inner diameter at the mid-height of the casting.

The LVDT results for the outer diameter are shown in Figure 14. A negative slope reflects contraction. Similar to the inner diameter measurements, most of the variation between the outer diameter curves occur in the first 400 s, after which the

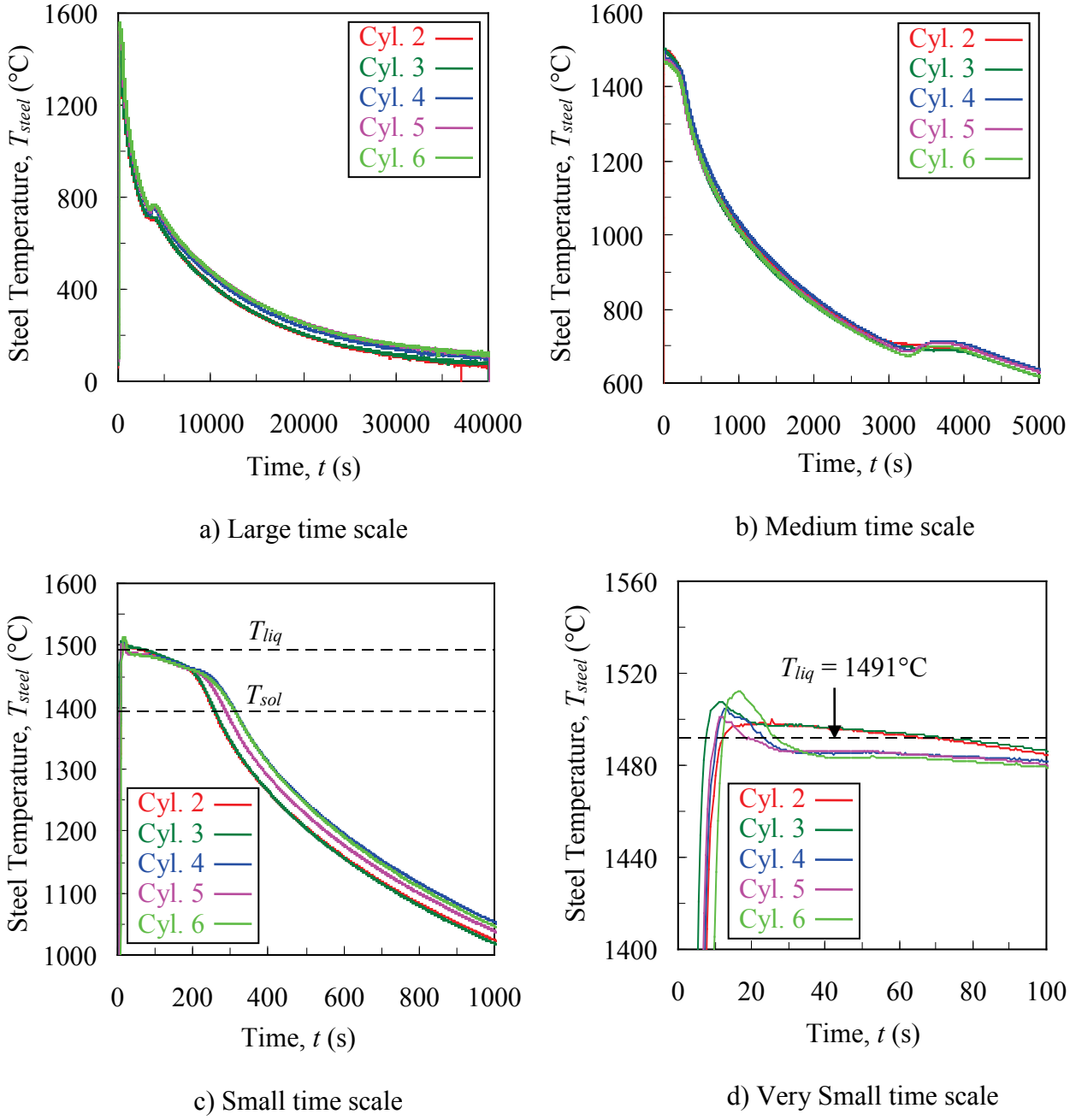

Figure 9. Temperature results in the steel. The Cylinder 1 thermocouple failed. The liquidus temperature was experimentally determined when the release of latent heat caused the temperature to become nearly constant with time (seen on the Very Small time scale).

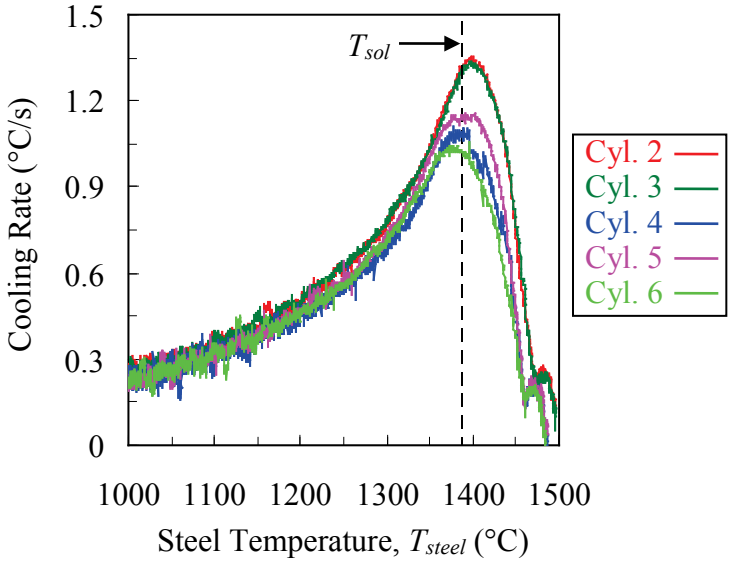

Figure 10. Cooling rates in the steel. The cooling rate is calculated as the differential temperature change during the recording time interval. The solidus temperature is experimentally determined at the maximum cooling rate.

curves are essentially parallel. This initial disagreement can again be attributed to mold expansion; immediately after pouring, the heat from the casting travels radially outward in the mold. This causes the sand near the mold-metal interface to expand. However, the region of the mold far from the interface (near the outer mold wall) is still cold and does not experience any expansion; in addition, this region is much stronger than the mold material near the casting, whose strength is significantly reduced after the binder evaporates. Thus, the sand expands inward into the mold cavity to cause an initial decrease in the outer diameter. This expansion is seen on the Small time scale as a decrease in the "outer 2" curve of 0.25 mm during the first 200s. Unfortunately, a similar decrease is not seen on the "outer 1" curve, which may be explained by relative movement between either 1) the quartz probe and protective sleeve (i.e., the probe was not firmly seated in the sleeve), or 2) the casting and protective sleeve, as the casting may have been mostly liquid and unable to firmly grasp the sleeve at these early times.

In addition to the LVDT results, measurements were also taken at several locations (termed feature lengths) from the pattern and casting (after shakeout) with a digital calipers. The resulting pattern allowances (PA) were calculated using the follow relation

$$PA = \frac{\left(feature\ \ length\right)_{initial} - \left(feature\ \ length\right)_{final}}{\left(feature\ \ length\right)_{initial}} \times 100 \qquad (1)$$

where $(feature\ \ length)_{initial}$ and $(feature\ \ length)_{final}$ are the caliper measurements taken from the pattern and casting (after shakeout), respectively. All pattern allowances are

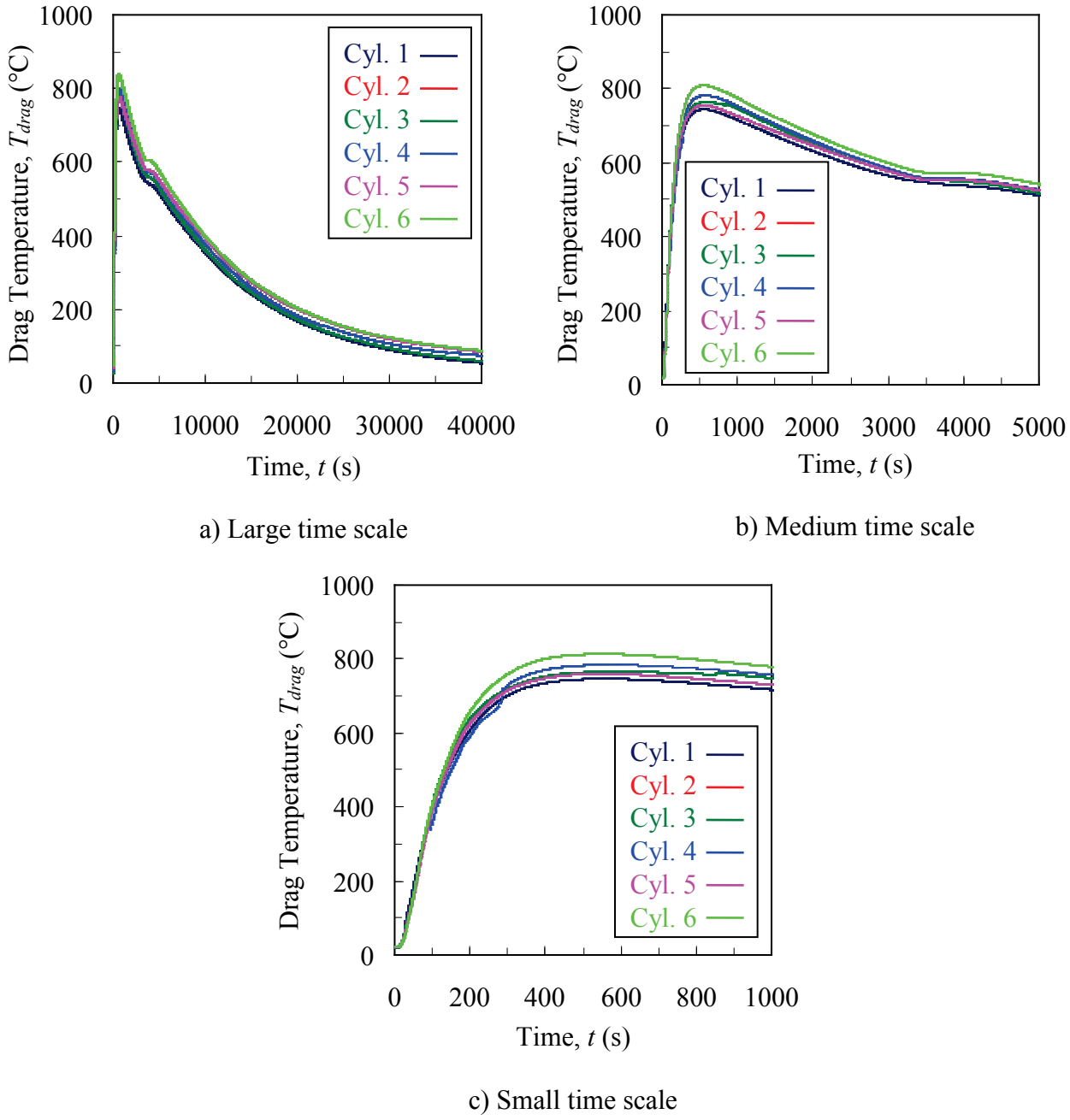

Figure 11. Temperature results in the drag.

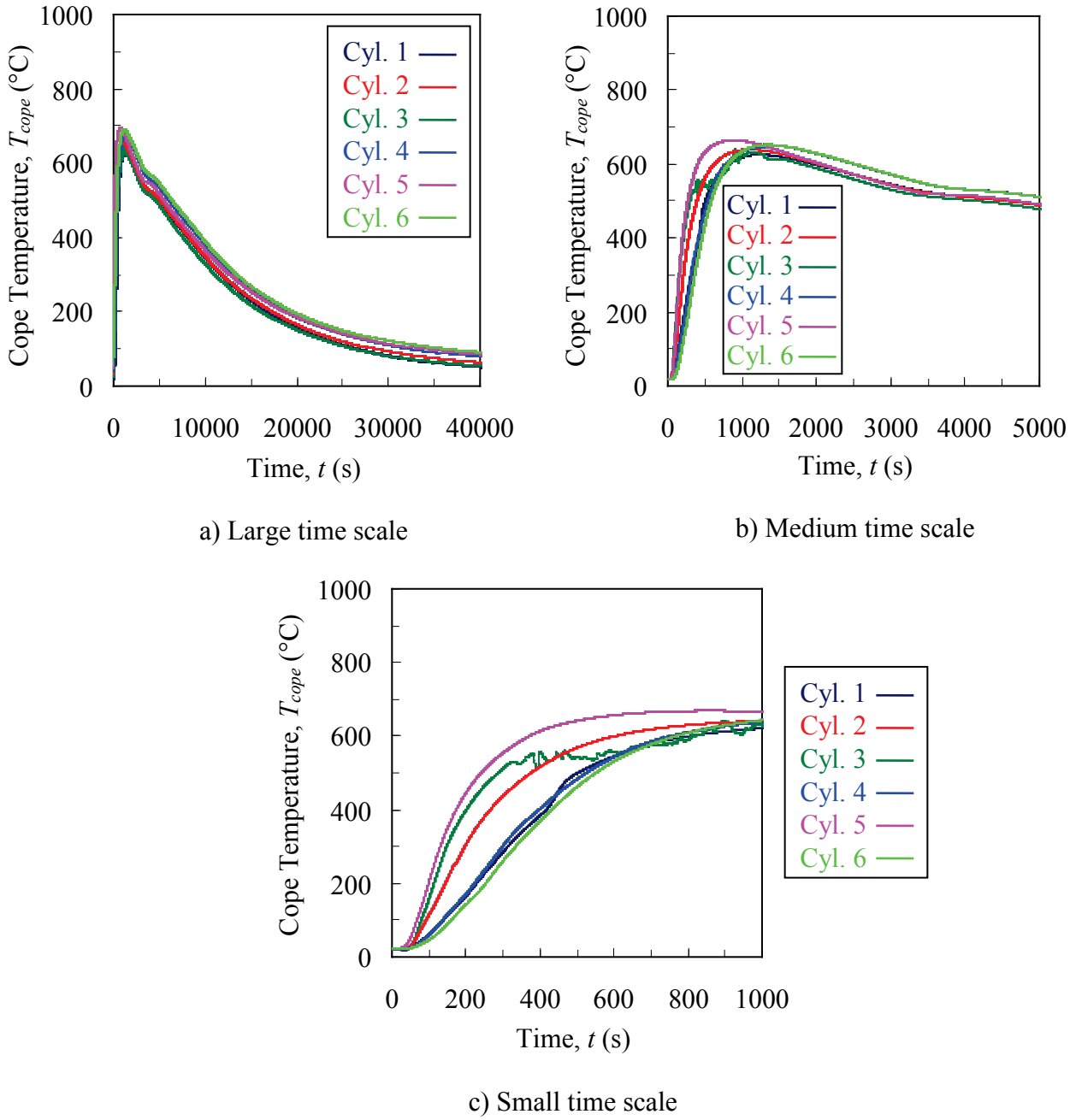

Figure 12. Temperature results in the cope.

reported as percentages, with a positive value reflecting contraction. In total, measurements of six feature lengths were taken, which include inner and outer diameter measurements at three casting heights (bottom, middle, top). The pattern allowances and feature length dimensions are summarized in Figure 15. This plot also includes the pattern allowances of the inner and outer diameters measured by the LVDT's, which were calculated by replacing the numerator in Equation 1 with the LVDT measurement at room temperature.

The caliper measurements at the mid-height of the inner diameter (ID_{mid}) were taken at the same location as the inner diameter LVDT measurements; thus, both pattern allowances (measured at room temperature) should agree. However, the calipers (circular symbols) measured an average pattern allowance of -1.9%, i.e., 1.9% expansion, while the LVDT's (triangular symbols) measured essentially no expansion. This disagreement is unfortunate but can be explained; recall from the inner diameter LVDT results (shown in Figure 13) that both curves are parallel after solidification. This experimental reproducibility suggests the validity of the LVDT measurements after 400 s. Therefore, the disagreement likely occurs before solidification is complete; this implies the previous assumption that the molten steel immediately solidifies around the protective sleeves is incorrect. Most likely, the semi-solid steel slipped on the sleeve during core expansion, resulting in relative translation between the quartz rod and casting that was not measured by the LVDT. The pattern allowances at the mid-height of the outer diameter (OD_{mid}) also show a variation (albeit, smaller than at ID_{mid}) between the caliper and LVDT measurements. Again, slippage between the protective sleeve and casting is a likely cause. The notion of slippage is also supported by the outer diameter LVDT measurements of Cylinder 1 (shown by the "outer 2" curve in Figure 14), as no change is measured until after 200 s.

Table 3 compares the dimensional changes measured by the calipers and LVDT's (at room temperature); while the inner diameter differences (approximately 1 mm) between the caliper and LVDT measurements may appear small, the resulting difference in the pattern allowances is nearly 2%.

In Figure 15(a), the average inner and outer pattern allowances at the bottom of the cylinder (ID_{bot} and OD_{bot}) are close to the free shrink of the steel (2.2%). Since the bottom of the casting cools faster, and thus, solidifies before the rest of the casting, the core no longer has sufficient strength to resist the contracting cylinder. It should also be noted that the outer mold expansion increases the outer diameter pattern allowances because the expansion is in the same radial direction as the cylinder contraction. Conversely, core expansion reduces the inner diameter pattern allowances, as the core expands in the opposite direction of the cylinder contraction. Hence, it is obvious that feature length affected most by mold expansion is the inner diameter at the mid-height (ID_{mid}). The average pattern allowance deviates from the free shrink line by a magnitude of 4%. The inner diameter pattern allowances at the top (ID_{top}) and bottom (ID_{bot}) are -0.3% and 1.9%, respectively. Therefore, the final inner diameter of the cylinder is barrel-shaped. For the outer diameter, the top (OD_{top}) and mid-height (OD_{mid}) diameter pattern allowances measured 3% and 2.7%, respectively. These values are slightly larger than the free shrink, again owing to mold expansion.

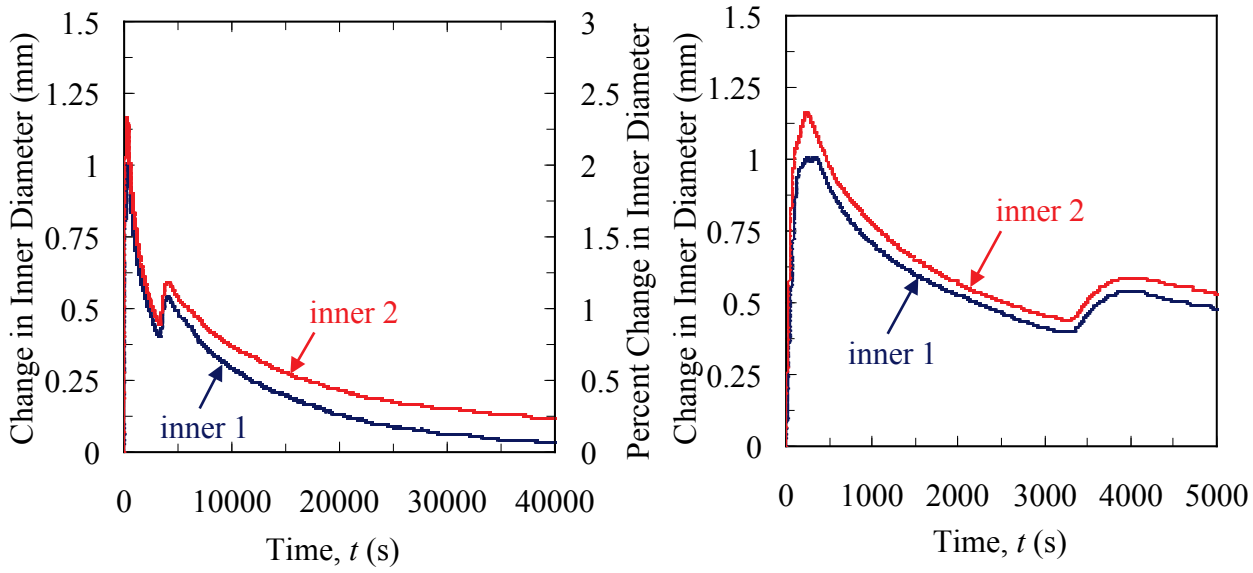

a) Large time scale

b) Medium time scale

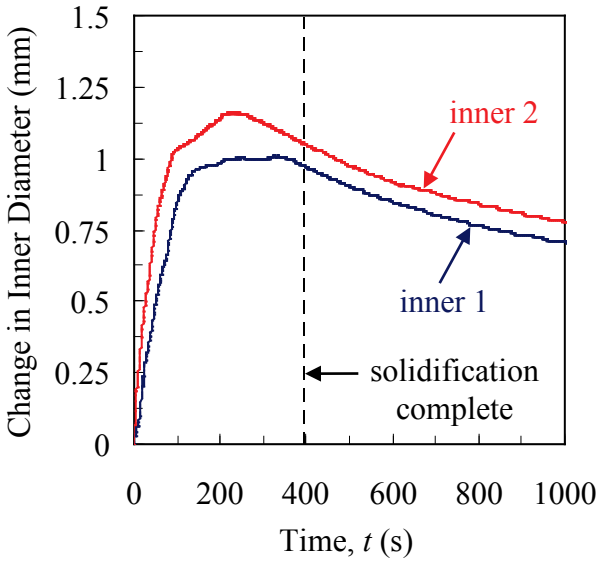

c) Small time scale

Figure 13. LVDT results for the change in inner diameter. The "inner 1" and "inner 2" curves are from the "Cylinder 4" and "Cylinder 5" experiments, respectively. The quartz rods failed in the "Cylinder 1" and "Cylinder 2" experiments. Positive change in the inner diameter is the result of core expansion.

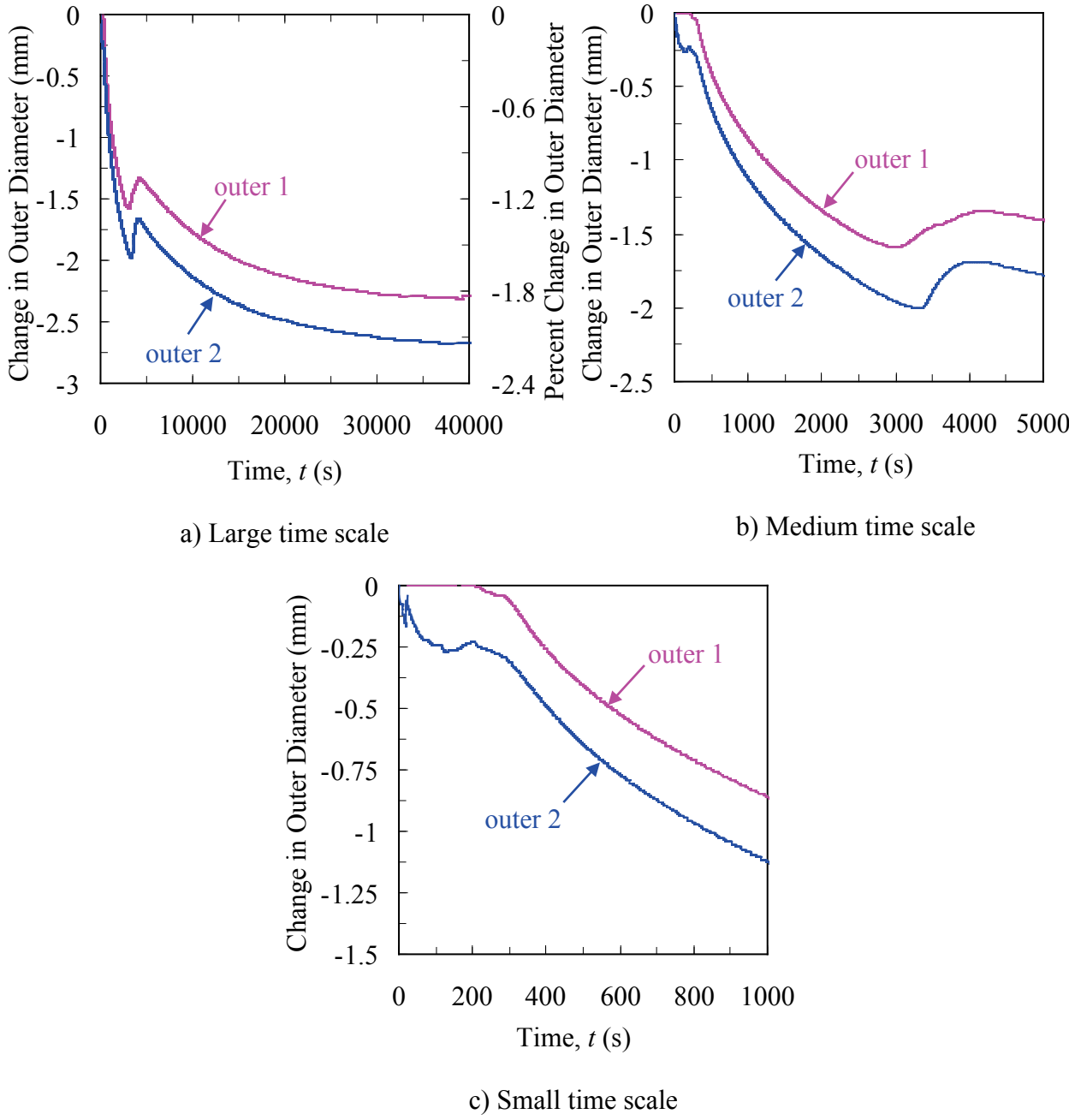

Figure 14. LVDT results for the change in outer diameter. The "outer 1" and "outer 2" curves are from the "Cylinder 1" and "Cylinder 4" experiments, respectively. A negative change in the outer diameter is the result of contraction.

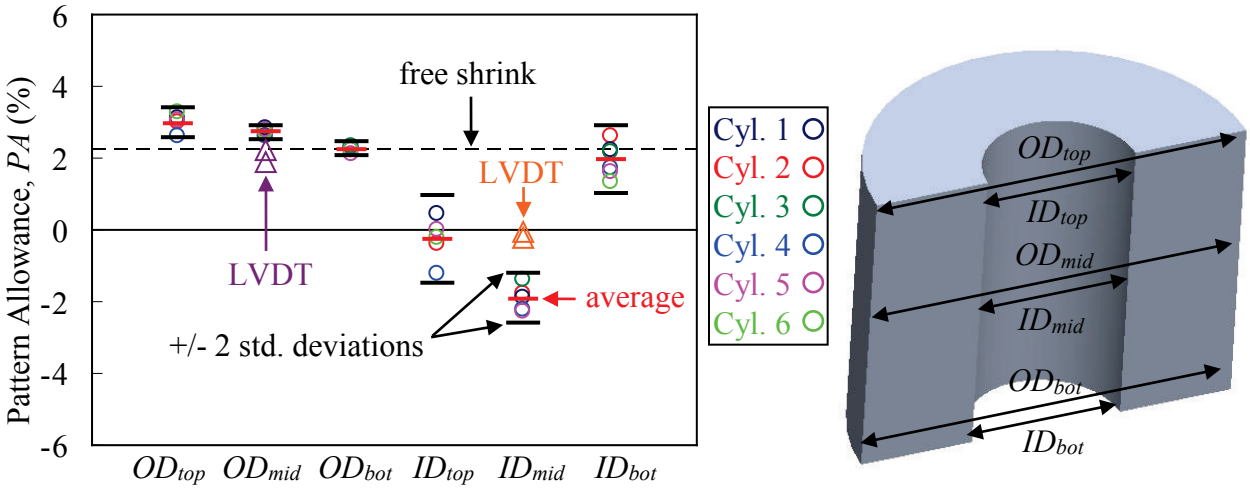

a) Pattern Allowance b) Description of Feature Lengths

Figure 15. Pattern allowances of feature lengths. Pattern allowances were calculated by the relation $PA = \{[(feature\ length)_{initial} - (feature\ length)_{final}]/(feature\ length)_{initial}\} \times 100$.

Table 3. Comparison of dimensional differences measured by LVDT's and calipers. All dimensions in mm.

	LVDT Room Temperature Value	Calipers
Inner Diameter 1	0.12	1.12
Inner Diameter 2	0.04	1.17
Outer Diameter 1	-2.31	-3.15
Outer Diameter 2	-2.72	-3.17

3. Thermal Simulations

Because a steel casting process occurs over a large temperature range, the material properties (of the mold and casting) are inherently temperature-dependent. In particular, the thermal expansion coefficient and constitutive model parameters vary with temperature. Therefore, the accurate calculation of temperatures is a necessary step in

the process of predicting casting distortions. Through an iterative process, the measured and simulated temperature temperatures were matched in both the steel and sand. This is a lengthy process which is not discussed here. For the interested reader, a detailed description of this procedure is given by Galles and Beckermann [6].

A comparison between simulated and measured temperatures in the steel is shown in Figure 16, for which excellent agreement was achieved at all times. Because thermal strains in the steel occur throughout the casting process, temperature agreement at all times in the steel is critical to the success of predicting thermal contractions.

The simulated temperatures in the drag and cope are compared with the measurements in Figures 17 and 18, respectively. While the simulated cope temperatures are also in good agreement with the measurements, the simulated drag temperatures agree with the measurements very well until 600 s, after which the simulation cools much faster than the measurement, shown in Figure 17(b). Recall from the LVDT measurements that the outer sand mold only appears to have an impact on the casting before solidification, which is complete for all experiments by 400 s. Therefore, the outer mold only requires consideration up to the solidification time. If the thermal strain simulations show that the outer mold impacts the casting beyond 600 s, additional thermal simulations may be required to achieve better agreement at later times.

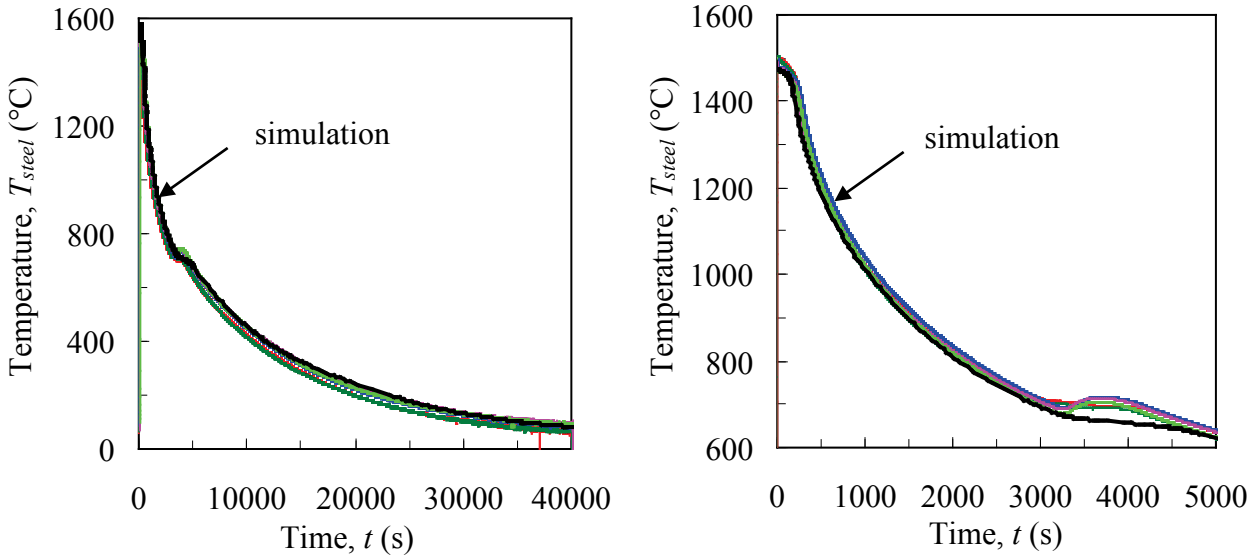

(a) Large time scale

(b) Medium time scale

Figure 16. Comparison between measured and simulated temperatures in the steel.

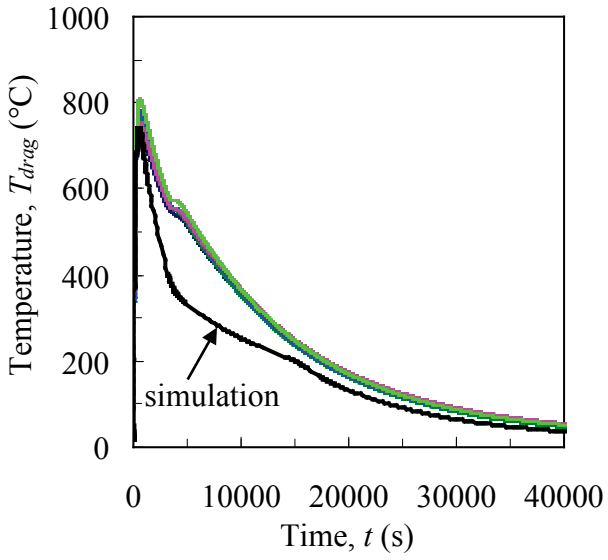

(a) Large time scale

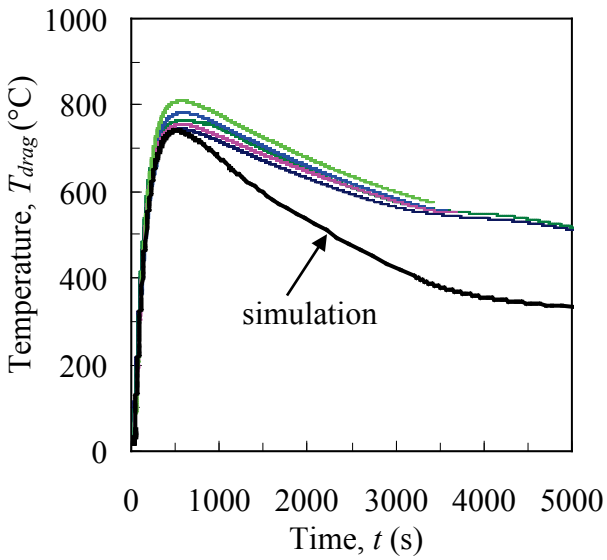

(b) Medium time scale

Figure 17. Comparison between measured and simulated temperatures in the drag.

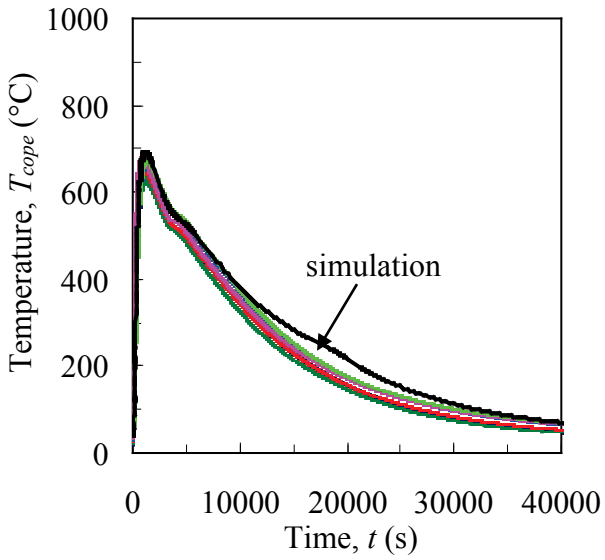

(a) Large time scale

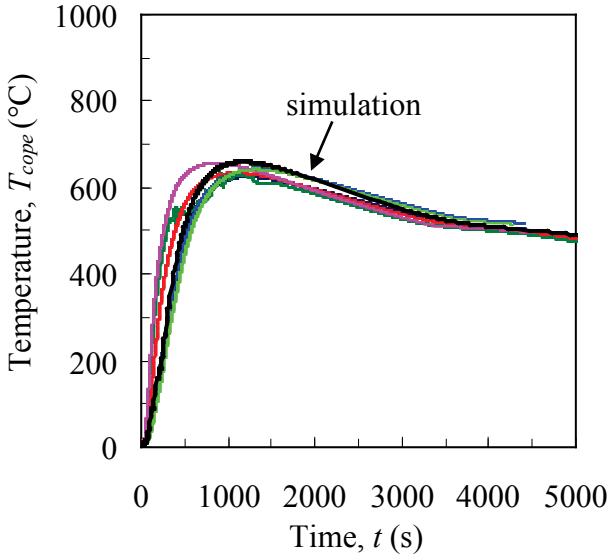

(b) Medium time scale

Figure 18. Comparison between measured and simulated temperatures in the cope.

4. Thermal Strains

Thermal (i.e., stress-free) expansions and contractions of the mold and cylinder are responsible for the majority of the dimensional changes throughout the casting process. Before calculating the stresses and distortions in the casting and core, it is constructive to compute the thermal expansion and contraction of the mold and cylinder. These preliminary calculations (performed in ABAQUS) will give insight to the critical times during the casting process when distortions are likely to occur. In addition, the accuracy of the thermal expansion coefficients will be validated.

Each component (core, outer mold, casting) was modeled separately in ABAQUS; to prevent the buildup of stresses, the elastic modulus was set to a very low value (1×10^{-8} MPa). Additionally, in order to realistically model expansion of the outer mold, zero-displacement boundary conditions were applied to the outer surfaces, which forced the mold expansion into the cavity. Temperature fields from MAGMAsoft were exported to the ABAQUS mesh at a sufficient number of time steps (130) to obtain a smooth temperature evolution at all locations.

The total linear thermal expansion coefficient (α_{tot}), which is required by ABAQUS to calculate the thermal strains, is related to the linear thermal expansion by

$$\alpha_{tot} = \frac{1}{\left(T - T_{ref}\right)} \int_{T_{ref}}^{T} \left(\frac{d\varepsilon}{dT}\right) dT \tag{2}$$

where T is the temperature, T_{ref} is the reference temperature at which thermal strain commences, and ε is linear thermal expansion. Additionally, the term $d\varepsilon/dT$ is the differential linear thermal expansion coefficient (α). Plots of the linear thermal expansion and total linear expansion coefficient for both the steel and mold are shown in Figure 19. The total linear thermal expansion coefficient of the steel (shown in Figure 19(b)), was calibrated to the experiments of Galles and Beckermann [3], from which the linear expansion curve was subsequently derived. The linear expansion curve of the mold was measured at the University of Northern Iowa's Metal Casting Center with a vertical, single push-rod controlled atmosphere dilatometer built by Theta Industries [7]; the total linear thermal expansion coefficient in Figure 19(b) was subsequently calculated using Equation 2.

The simulated outer diameter (OD) core expansion and cylinder contraction at the inner diameter are shown in Figures 20 and 21, respectively. Because the core is in contact with the cylinder throughout the casting process, the outer diameter of the core is coincident with the inner diameter of the cylinder at all times; therefore, they can be directly compared with each other. At the time of complete solidification, the OD core expansion (shown in Figure 20) was predicted to increase the inner diameter by only 0.5 mm at the mid-height of the cylinder, which is significantly less than the measured expansion of 1 mm. This discrepancy may be due to an incorrect coefficient of thermal expansion for the mold. Therefore, a parametric study was conducted to illustrate how an adjustment to the total linear thermal expansion coefficient would impact the core expansion before solidification. For the study, it was assumed that the lower-temperature coefficient values ($T < 600$°C), which are very similar to those measured by Andrews [8],

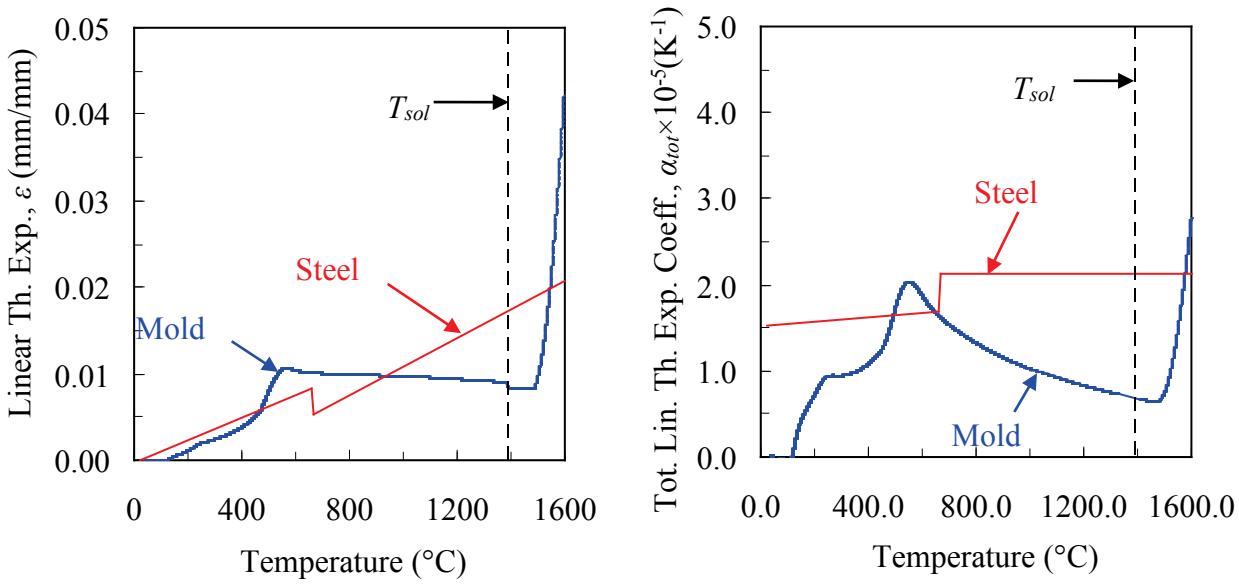

(a) Linear Thermal Expansion

(b) Total Linear Thermal Expansion Coefficient

Figure 19. Linear thermal expansion and total linear thermal expansion coefficient of the mold and steel. The total linear thermal expansion coefficient is calculated from the linear thermal expansion using Equation 2.

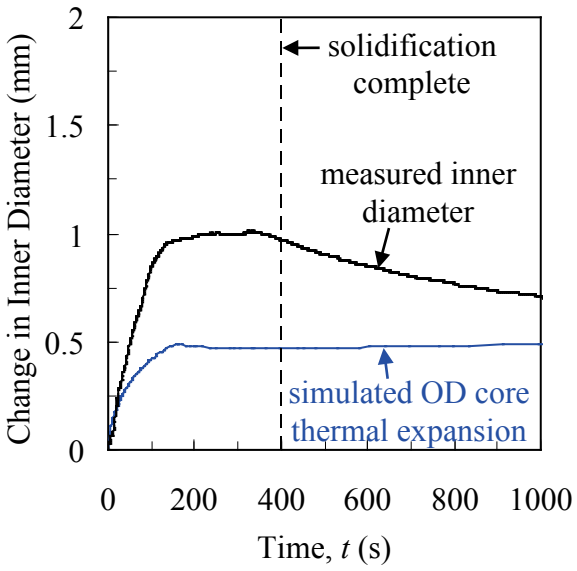

Figure 20. Simulated outer diameter (OD) core thermal expansion. The outer diameter of the core is coincident with the inner diameter of the cylinder at all times. At the time of complete solidification, the core expansion is predicted to increase the inner diameter by only 0.5 mm, which is significantly less than the measured expansion of 1 mm. This discrepancy may be due to an incorrect coefficient of thermal expansion for the mold.

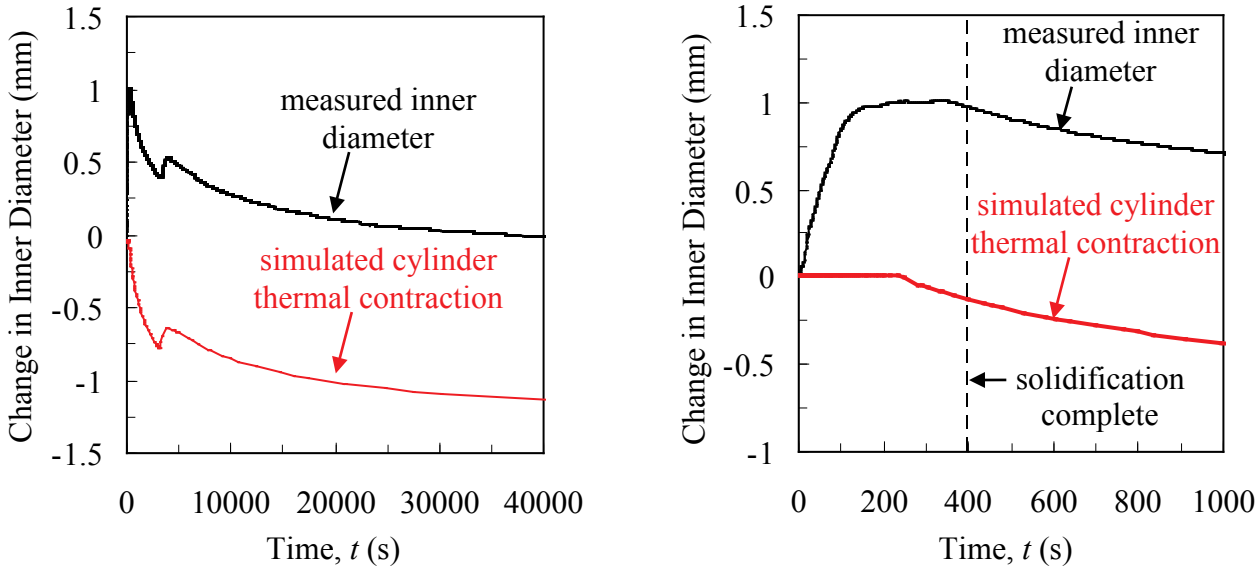

(a) Large Time Scale

(b) Small Time Scale

Figure 21. Simulated cylinder thermal contraction at the cylinder inner diameter. The "simulated cylinder contraction" curve is parallel to the measured inner diameter curve at all times after 400 s, suggesting that all dimensional changes after solidification are the result of thermal contraction in the cylinder.

are accurate and should not be adjusted. Therefore, the total linear thermal expansion coefficient was only adjusted at high temperatures, as shown in Figure 22(b). Adjustment 1 resulted a core thermal expansion of approximately 1 mm after 200 s. While the simulated expansion matches magnitude of the measured inner diameter expansion, the rate of expansion is less than the measured rate, i.e., the initial slope of the "measured inner diameter" curve is steeper than the "adjustment 1" curve. Assuming core distortions have a negligible effect on dimensional changes of the inner diameter at early times (t < 100 s), the total linear thermal expansion coefficient must be further adjusted to match the initial slope of the inner diameter. This was accomplished using the "adjustment 2" curve in Figure 22(b), which resulted in excellent agreement between the slopes of the "adjustment 2" and "measured inner diameter" curves. The "adjustment 2" curve continues to increase to a value of 1.8 mm at 200 s. However, at some time before solidification, the steel reaches coherency, after which the core cannot expand freely. This may explain the (nearly) constant slope of the "measured inner diameter" curve after 100 s, as the strengthening steel impedes core expansion. The time at which this occurs will be determined after implementation of the mechanical model.

The "simulated cylinder contraction" curve in Figure 21 is parallel to the measured inner diameter curve at all times after 400 s. This confirms that all dimensional changes after (or shortly after) solidification are the result of thermal contraction in the cylinder.

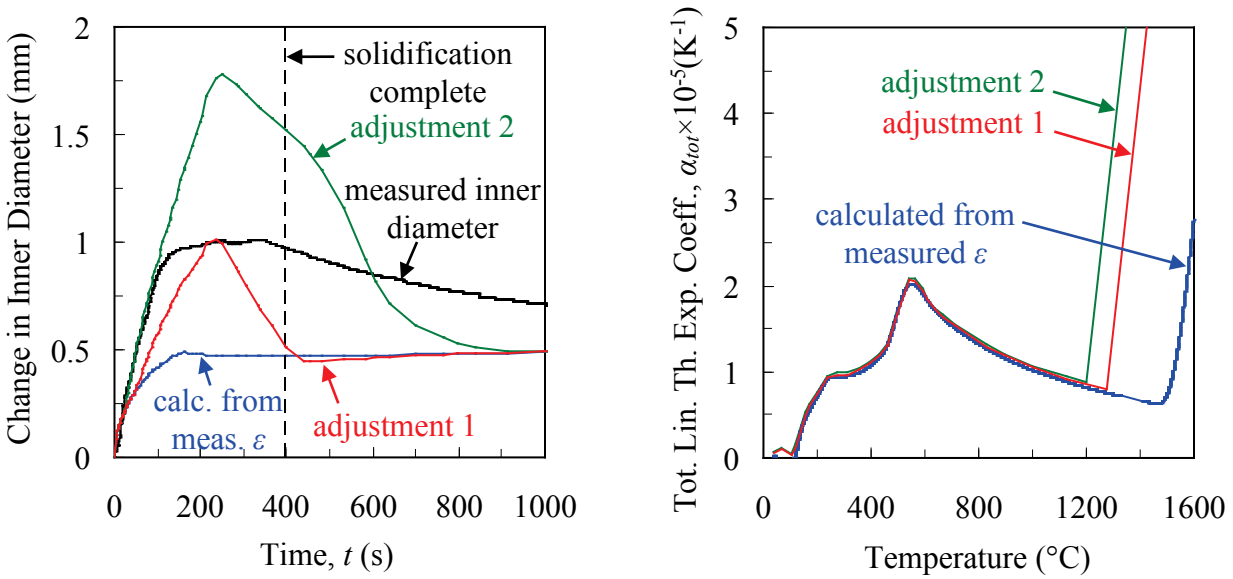

(a) Simulated Core Expansion

(b) Total Linear Thermal Expansion Coefficient of Mold

Figure 22. Simulated outer diameter (OD) core thermal expansion after adjustments to the total linear thermal expansion coefficient. The outer diameter of the core is coincident to the inner diameter of the cylinder at all times. The simulated OD core expansion using the total thermal expansion coefficient (calculated from the measured mold ε in Figure 19(a)) was not large enough to account for the initial measured expansion of the inner diameter. A parametric study shows adjustments to the total thermal expansion coefficient at higher temperatures has a large impact on the simulated core expansion before solidification.

The simulated mold thermal expansion and cylinder thermal contraction at the outer diameter are shown in Figures 23 and 24, respectively. The initial decrease in the "simulated mold thermal expansion" curve to a value of -0.25 mm at 200 s shows the ability of the simulation to predict mold expansion into the mold cavity. After 300 s, the measured outer diameter decreases at a higher rate than the simulated expansion of the mold; as a result, an air gap forms and the casting no longer mechanically interacts with the outer mold. Before 300 s, however, the mold and casting are likely in contact, which introduces the possibility of distortions. At this time, it is unclear as to whether the outer mold expansion can generate the magnitude of stresses required for plastic deformation. Again, implementation of the mechanical model will determine when the solidifying casting has gained sufficient strength to resist mold expansion, which could result in distortions.

The simulated thermal contraction of the cylinder at the outer diameter is very similar to the simulated inner diameter contraction (shown in Figure 21), as the measured and simulated curves in Figure 24 are parallel after 400 s, indicating free contraction. The curves do appear to converge somewhat after 25000 s; however, this is likely due to some error in the thermal simulations.

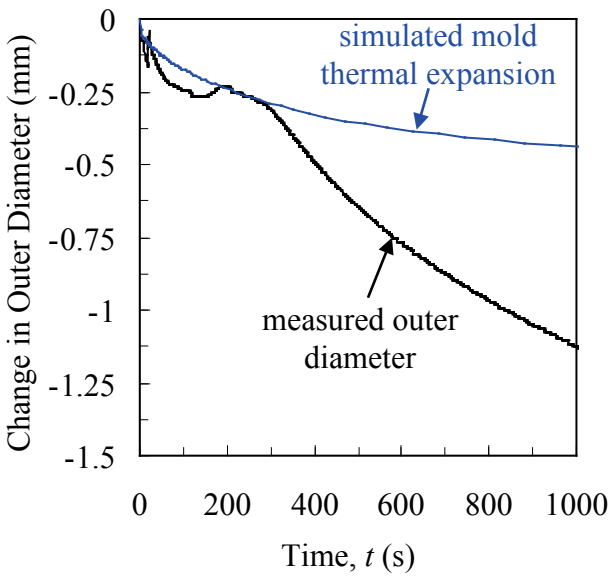

Figure 23. Simulated mold thermal expansion at the cylinder outer diameter. The decrease in the "simulated mold thermal expansion" curve to -0.25 mm after 200 s demonstrates the ability of the simulation to predict outer mold expansion into the mold cavity.

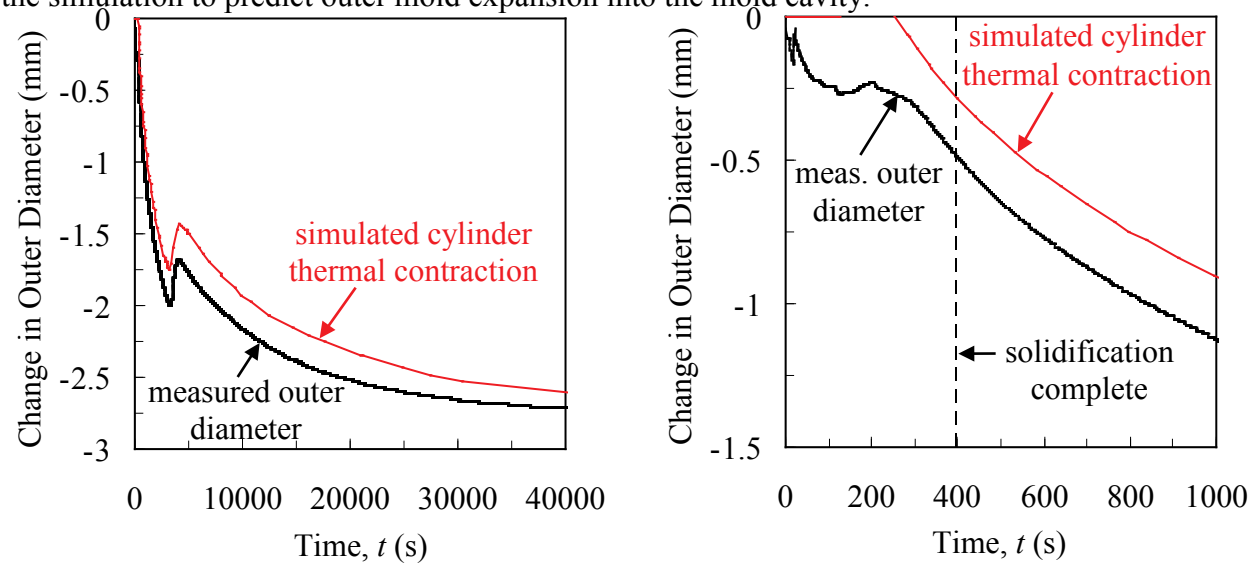

a) Large Time Scale

b) Small Time Scale

Figure 24. Simulated cylinder thermal contraction at the cylinder outer diameter. Similar to the cylinder thermal contraction at inner diameter, the outer diameter "simulated cylinder thermal contraction" curve is essentially parallel to the measured outer diameter after 400 s, suggesting that all dimensional changes after solidification are the result of thermal contraction in the cylinder.

5. Conclusions and Future Work

The present work studied the effect of a core on casting distortions of a low-carbon steel cylinder. A thick-walled cylinder was produced in a series of casting experiments, in which the inner and outer diameters were continuously measured with LVDT's. Additional measurements (taken with a digital calipers) revealed a barrel-shaped final inner diameter, as the mid-height diameter increased significantly due to core expansion. However, differences in dimensional changes measured by the calipers and LVDT at the same location suggest the quartz probes (which translated the casting displacement to the LVDT) slipped relative to the cylinder before the steel reached coherency. Thermal strain simulations were performed in ABAQUS; the results indicated 1) an adjustment to the thermal expansion coefficient of the mold is needed at high temperatures and 2) all dimensional changes in the casting after solidification are due to thermal contractions of the steel. Future work includes 1) improving the experimental setup to successfully measure the initial mold expansion with LVDT's and 2) implementing mechanical models of both the mold and casting to predict casting distortions.

Acknowledgements

This research is sponsored by the DLA – Troop Support, Philadelphia, PA and the Defense Logistics Agency Logistics Operations, J335, Research & Development, Ft. Belvoir, VA. Additional thanks to Jerry Thiel and the students from the Metal Casting Center at the University of Northern Iowa for their assistance with the casting experiments.

References

1. P.J. Wray, Effect of carbon content on the plastic flow of plain carbon steels at elevated temperatures, *Metallurgical Transactions A*, vol. 13A, no. 1, pp 125-34, 1982.

2. T. Suzuki, K.H. Tacke, K. Wunnenberg, and K. Schwerdtfeger, Creep properties of steel at continuous casting temperatures, *Ironmaking and Steelmaking*, vol. 15, no. 2, pp 90-100, 1988.

3. D. Galles, C. Monroe, and C. Beckermann, Measurement and prediction of stresses during casting of a steel bar, *Proceedings of the 65th SFSA Technical and Operating Conference*, Paper No. 5.5, Steel Founders' Society of America, Chicago, IL 2011.

4. *MAGMAsoft*, MAGMA GmbH, Kackerstrasse 11, 52072 Aachen, Germany.

5. *Abaqus/Standard*, Abaqus, Inc., Providence, RI, 2006.

6. D. Galles and C. Beckermann, Measurement and simulation of distortion of a steel bracket casting, *Proceedings of the 66th SFSA Technical and Operating Conference*, Paper No. 5.2, Steel Founders' Society of America, Chicago, IL 2012.

7. *Theta Industries*, Theta Industries Inc., Port Washington, NY, 11050.

8. J.B. Andrews, R.N. Andrews, and D. Swain, SFSA Research Report 102A, Des Plaines, IL, USA, Steel Founders' Society of America, 1990.